THE JOURNAL OF PHYSICAL CHEMISTRY A

Article

pubs.acs.org/JPCA

Insight into Magnesium Coordination Environments in Benzoate and Salicylate Complexes through ^{25}Mg Solid-State NMR Spectroscopy

Kevin M. N. Burgess, Yang Xu, Matthew C. Leclerc, and David L. Bryce*

Department of Chemistry and Centre for Catalysis Research and Innovation, University of Ottawa, 10 Marie Curie Private, Ottawa, Ontario, Canada K1N 6N5

Supporting Information

ABSTRACT: We report on the ^{25}Mg solid-state nuclear magnetic resonance (NMR) characterization of a series of magnesium complexes featuring Mg^{2+} ions in organic coordination environments. Six compounds have been synthesized with benzoate and salicylate ligands, which are typically used as linkers in metal organic frameworks (MOFs). The use of ultrahigh-field solid-state NMR has revealed a relatively large range of values for the ^{25}Mg quadrupolar coupling constant, $C_Q(^{25}Mg)$, in these compounds. In contrast to some previously studied inorganic Mg^{2+} complexes, the values of $C_Q(^{25}Mg)$ in organic Mg^{2+} complexes are well rationalized by the degree of octahedral strain of the "MgO_6" coordination polyhedra. ^{13}C and ^{25}Mg isotropic chemical shifts were also found to be sensitive to the binding mode of the carboxylate ligands. The experimental findings are corroborated by gauge-including projector-augmented-wave (GIPAW) density functional theory (DFT) computations, and these have allowed for an interpretation of the experimentally observed trend in the $C_Q(^{25}Mg)$ values and for the visualization of the EFG tensor principal components with respect to the molecular structure. These new insights may prove to be valuable for the understanding and interpretation of ^{25}Mg NMR data for Mg^{2+} ions in organic binding environments such as those found in MOFs and protein-divalent metal binding sites.

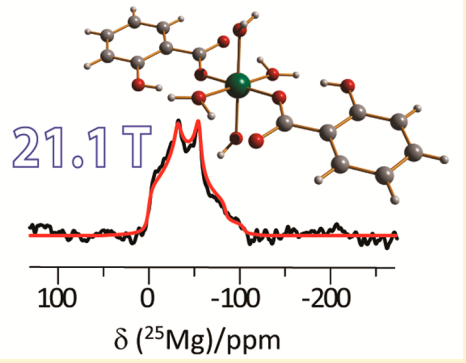

INTRODUCTION

The divalent magnesium cation (Mg^{2+}) plays an essential role in many biochemical processes as well as in materials science.[1,2] Very recently, there has been substantial interest in the synthesis and characterization of metal organic frameworks (MOFs) comprising affordable metals such as the alkaline-earth metals, including magnesium.[3−6] Insight into the local structure and coordination environment surrounding the Mg^{2+} cation is important if we wish to understand how magnesium can play a role in future materials science applications in general. Analytical methods currently available to gain site-specific information on the coordination polyhedra about Mg^{2+} in the solid state are rare.[7] It is known that solid-state nuclear magnetic resonance (SSNMR) parameters are sensitive to small structural changes about the probed nucleus.[8−10] This has opened the door to the possibility of "NMR crystallography",[11] where crystal structures can be refined[12−15] or fully solved with both SSNMR and powder X-ray diffraction (PXRD).[16−24] The only NMR-active isotope of magnesium is the quadrupolar (i.e., spin quantum number, I, is greater than 1/2) ^{25}Mg nucleus (I = 5/2), with a natural abundance of 10.1%. The central transition (CT, $m = +1/2 \leftrightarrow -1/2$) NMR spectra are complicated due to the anisotropic broadening caused by the second-order quadrupolar interaction (QI) for half-integer quadrupolar nuclei such as ^{25}Mg. The QI is the coupling between the quadrupole moment (for ^{25}Mg, Q = 199.4 mb)[25] and the electric field gradient (EFG) at the magnesium nucleus. The QI may be characterized by a traceless second-rank tensor which is parametrized by the quadrupolar coupling constant, C_Q, and an asymmetry parameter, η_Q. The QI typically acts as a perturbation to the Zeeman splitting once the nucleus is placed in a magnetic field of strength B_0. ^{25}Mg is considered a low-γ nucleus owing to its small magnetogyric ratio (at 9.4 T, $\nu_L(^{25}Mg)$ = 24.5 MHz).

Advances in NMR technology have allowed for the development of ultrahigh-field magnets (B_0 > 18.8 T), thus making the study of the challenging ^{25}Mg nucleus increasingly feasible. However, studies to date have been mainly focused on inorganic materials such as oxides, silicates, and phosphates.[26] For example, Laurencin and co-workers[27] recently recorded high-quality ^{25}Mg SSNMR spectra for a series of magnesium phosphates in magnetic fields of 17.6 and 20.0 T and have attempted to use their benchmark ^{25}Mg SSNMR data to aid in the characterization of magnesium-doped hydroxyapatite [$Ca_{9.1}Mg_{0.9}(PO_4)_6(OH)_2$], a material found in bone and teeth. However, it is apparent that there is a dearth of ^{25}Mg SSNMR studies of Mg^{2+} in organic molecular environments as highlighted by Smith and co-workers in a recent review;[26] they state that "the accumulation of a larger number of reliable NMR data in Mg-containing organic materials is certainly required for

Received: May 24, 2013
Revised: July 2, 2013
Published: July 8, 2013

the establishment of meaningful and useful correlations between the ^{25}Mg NMR parameters and structural aspects of the bonding involving Mg^{2+}". In addition to the difficulties associated with all ^{25}Mg NMR studies noted above, one of the main reasons for the lack of ^{25}Mg SSNMR data for organic systems is the low mass-percentage of magnesium present in them, resulting in challenges in obtaining spectra with acceptable signal-to-noise ratios. Such difficulties have led to the use of somewhat costly ^{25}Mg isotopic enrichment schemes[28] such as in the cases of Mg(TTP)·Py_2 (TTP = 5,10,15,20-tetraphenylporphyrinato)[29] and magnesium phthalocyanine (MgPc·H_2O·Py).[30] Lipton et al.[31] have used isotopic enrichment along with ^{1}H→^{25}Mg cross-polarization at very low temperatures (10 K) to investigate the binding modes of Mg^{2+} (0.07% by weight) in the DNA repair protein apurinic/apyrimidic endonuclease 1 (AEP1). Simultaneously, sensitivity enhancement methods that manipulate nuclear satellite populations in favor of enhancing the CT population difference[32] such as hyperbolic secant (HS)[33] or double frequency sweeps (DFS)[34−36] or the quadrupolar Carr−Purcell−Meiboom−Gill (QCPMG)[37,38] pulse sequence have enabled the characterization of a handful of octahedral "MgO_6" environments such as those found in magnesium acetate, acetylacetonate, and formate.[39,40] With an eye to application in characterizing magnesium-based MOFs and other Mg^{2+}-binding organic and biochemical compounds, it is therefore desirable to acquire reliable ^{25}Mg SSNMR data for a larger set of organic complexes with known structure to establish useful relationships between the ^{25}Mg NMR parameters and the immediate coordination environment surrounding Mg^{2+} in such systems.[26]

In this study we have synthesized six magnesium benzoates and salicylates where the structures of the ligands are found in Scheme 1, and for which crystal structures are known from X-ray diffraction.[41] These are an important class of ligands given the utility of benzoates as common backbones in many MOFs used, for example, for the adsorption of gases such as CO_2.[42] Very recently, Huang and co-workers probed Mg^{2+} centers via ultrahigh-field ^{25}Mg SSNMR in the CPO-27-Mg[43] and α-$Mg_3(HCOO)_6$[44] MOFs upon the adsorption of solvent vapors such as water, acetonitrile, acetone, dimethylformamide, and benzene. In both of these studies, it was not obvious how the NMR parameters (i.e., a range of 0.9 to 6.4 MHz in the $|C_Q(^{25}Mg)|$ values) are related to the fine details of the coordination environment about Mg. Although the complexes in the present work lack the extended three-dimensional network structures needed to be considered MOFs, they are nonetheless representative of various Mg MOFs both chemically, i.e., the nature of the Mg^{2+} coordination environments, and from a technical NMR standpoint, i.e., the number of ^{25}Mg nuclei per nm^3 of the solid (0.45 for CPO-27-Mg, 0.73 for α-$Mg_3(HCOO)_6$, and only 0.12 for Mg(p-NH_2sal) in this work). This systematic investigation will allow for more meaningful correlations regarding the relationship between ^{25}Mg NMR parameters and octahedral MgO_6 coordination environments in organic systems such as MOFs. Our interpretation of the NMR data will be aided by the use of gauge-including projector-augmented-wave (GIPAW) density functional theory (DFT), which has found widespread usage for the calculation of NMR parameters in solids.[45,46]

Scheme 1. Benzoate and Salicylate Ligands Used in This Study: ben (benzoate), *p*F (*p*-fluorobenzoate), *p*Cl (*p*-chlorobenzoate), sal (salicylate), *p*NH_2sal (*p*-aminosalicylate), and *p*NO_2 (*p*-nitrobenzoate)

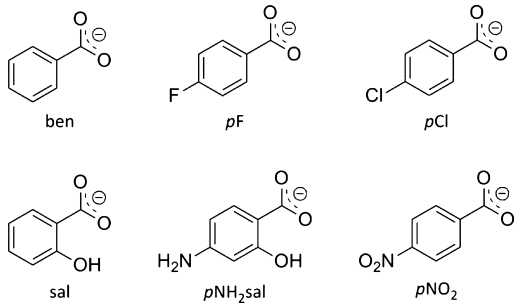

EXPERIMENTAL DETAILS

Sample Preparation. The materials necessary for the synthesis of the magnesium carboxylates (p-fluorobenzoic acid (pF), p-chlorobenzoic acid (pCl), p-nitrobenzoic acid ($p$$NO_2$), sodium benzoate (Na(ben)), sodium salicylate (Na(sal)), sodium p-aminosalicylate (Na($p$$NH_2$sal)), magnesium carbonate ($MgCO_3$), and magnesium chloride ($MgCl_2$)) were all purchased from Sigma-Aldrich. All samples were prepared with ^{25}Mg at natural abundance.

Mg(pCl) and Mg($p$$NO_2$) were synthesized via a variation of a previously reported method by Arlin et al.[41] whereby a 1:1 stoichiometric mixture of 1 g of pCl or $p$$NO_2$ and the appropriate amount of $MgCO_3$ are first dissolved in 20 mL of distilled water. The solution is stirred overnight after which the nondissolved starting material is filtered over a pad of Celite. The collected colorless mother liquor is slowly evaporated at room temperature for several days until crystals of the appropriate Mg salt are obtained.

For Mg(ben), Mg(sal), and Mg($p$$NH_2$sal), 1 g of the apposite sodium salt was dissolved in a minimum of water to which the appropriate amount of $MgCl_2$ is added to reach a 1:1 stoichiometric ratio. The mixture was stirred for several minutes and then filtered through cotton. The resulting homogeneous solution was allowed to slowly evaporate over several days until transparent crystals appeared in the flask. A new crystal structure for Mg(ben) was acquired in the course of this study. The procedure for this and a complete table of X-ray data are given in the Supporting Information.

Mg(pF) cannot be synthesized in pure form in the same way as Mg(pCl) or Mg($p$$NO_2$). Thus, 1 g of ($p$F) was dissolved in 20 mL of EtOH to which 1 equiv of NaOH was added, and the mixture was refluxed for 1 h. The solvent was then evaporated, and 1 g of the resulting sodium salt was dissolved in a minimum of water to which the appropriate amount of $MgCl_2$ was added for a 2:1 stoichiometric ratio of Na(pF) to $MgCl_2$. This solution was filtered over cotton, and the collected mixture was allowed to evaporate slowly at room temperature where crystals of pure Mg(pF) formed within a few days.

All samples were ground into fine powders with a mortar and pestle for powder X-ray diffraction experiments and subsequently packed into 4 or 7 mm ZrO_2 rotors for solid-state NMR experiments.

Solid-State NMR Experiments. For ^{13}C solid-state NMR experiments, spectra were recorded at B_0 = 4.7 (Bruker AVANCE III, $\nu_L(^1H)$ = 200.13 MHz and $\nu_L(^{13}C)$ = 50.31 MHz) and 9.4 T (Bruker AVANCE III, $\nu_L(^1H)$ = 400.13 MHz and $\nu_L(^{13}C)$ = 100.62 MHz) using Bruker 4 mm (9.4 T) and 7 mm (4.7 T) triple-resonance (HXY) probes at the University of

dx.doi.org/10.1021/jp405145b | J. Phys. Chem. A 2013, 117, 6561−6570

Ottawa under cross-polarization/magic-angle spinning (CP/MAS) conditions. Individual experimental parameters along with chemical shift assignments for Mg aryl carboxylates are presented in the Supporting Information. Dipolar dephasing experiments[47] at B_0 = 4.7 T used a 40 μs delay between the pulse and the signal acquisition.

^{25}Mg solid-state NMR spectra were recorded at 9.4 T (Bruker AVANCE III, $\nu_L(^1H)$ = 400.13 MHz and $\nu_L(^{25}Mg)$ = 24.49 MHz) at the University of Ottawa and at 21.1 T (Bruker AVANCE II, $\nu_L(^1H)$ = 900.13 MHz and $\nu_L(^{25}Mg)$ = 55.10 MHz) at the National Ultrahigh-Field NMR Facility for Solids in Ottawa. At B_0 = 9.4 T, Bruker 7 mm static and MAS low-frequency double-resonance (HX) probes were used. At B_0 = 21.1 T, a Bruker 4 mm MAS low-frequency double-resonance (HX) probe, a Bruker 7 mm MAS low-frequency single-channel probe, and a 7 mm static home-built low-frequency double-resonance (HX) probe were used. Chemical shifts were referenced to a saturated aqueous solution of $MgCl_2$ at 0.0 ppm;[39] this solution was also used for pulse calibration. The CT-selective $\pi/2$ pulse for Mg aryl carboxylates was that of $MgCl_2$(aq) scaled by a factor of $1/(I + 1/2) = 1/3$ for ^{25}Mg. Spectra were acquired using either a solid echo (i.e., $\pi/2-\tau_1-\pi/2-\tau_2-$acq)[48] or Hahn-echo (i.e., $\pi/2-\tau_1-\pi-\tau_2-$acq)[49] sequence. At 9.4 T, it was sometimes necessary to use the double frequency sweeps (DFS)[34] polarization method to enhance the signal of the CT. In those cases, the DFS pulse swept from 800 to 80 kHz for a duration of 5 ms. In the case of Mg(sal), an enhancement of 2.5 was observed compared to the spectrum acquired without DFS. For Mg(sal), the QCPMG pulse sequence[37] was used to increase the signal-to-noise ratio of the spectrum. In this case, and in that of Mg(pNH$_2$sal), the variable offset cumulative spectra (VOCS) method[50] was needed to observe a uniform excitation profile. Specific experimental details for each compound are given in Table S4 of the Supporting Information.

Data Processing and Simulations. All spectra were processed using the Bruker TopSpin software (ver. 3.0). Echoes were left shifted whenever necessary and then Fourier transformed. ^{25}Mg NMR spectra were simulated with the WSolids[51] software package or, in the case of Mg(pCl), SIMPSON (with the zcw17710 crystallite file for powder averaging).[52] Some figures were generated with graphics produced by DMFit (version 2011).[53]

GIPAW DFT Calculations. GIPAW DFT computations were performed using version 4.1 of CASTEP-NMR (Accelrys Inc. San Diego, CA). Input files were generated via the Materials Studio version 3.2 software package (Accelrys Inc.)[54] with the available crystallographic information files (i.e., ref 41 for Mg(pF), Mg(pCl), and Mg(pNO$_2$); ref 58 for Mg(sal); ref 57 for Mg(pNH$_2$sal)). The exchange-correlation functional of Perdew, Burke, and Ernzerhof (PBE)[55] was used under the generalized gradient approximation (GGA) along with on-the-fly generated pseudopotentials. All hydrogen positions were optimized prior to NMR calculations, and so it was sometimes necessary to use the "coarse" setting for the energy cutoff, E_{cut}, and k-point grid settings for certain calculations due to the large unit cell volumes. Specific computational details for each compound discussed in this work can be found in Table S5 of the Supporting Information. ^{25}Mg magnetic shielding (MS) and EFG tensor information can be obtained from the generated .magres output files with a modified version of the EFGShield program.[56] The calculated shielding constants may be related to the value of δ_{iso} in the following way:

$$\delta_{iso} = (\sigma_{iso,ref} - \sigma_{iso})/(1 - \sigma_{iso,ref})$$

where $\sigma_{iso,ref}$ is the absolute shielding constant (566.1 ± 1.0 ppm) for ^{25}Mg.[40] Because of a doubly disordered water molecule in the lattices of Mg(ben) and Mg(pCl), two separate calculations were performed for each compound to examine the effects of the disorder on the MS and EFG tensor parameters.

RESULTS AND DISCUSSION

Synthesis and Initial Characterization. The X-ray crystal structures of Mg(pF), Mg(pCl), Mg(ben), and Mg(pNO$_2$) have been previously reported by Arlin et al.,[41] and slightly older structures are available for Mg(pNH$_2$sal)[57] and Mg(sal).[58] Because our ^{25}Mg NMR data were not consistent with the reported structure for Mg(ben), we have acquired a new crystal structure for this compound (vide infra). To verify the purity of the synthesized magnesium aryl carboxylates, we performed powder X-ray diffraction (PXRD) on each of the samples (see Figure S1 in the Supporting Information) to compare with the powder pattern predicted from the available crystal structures. As for Mg(pF), the proposed synthetic route[41] (1:1 $MgCO_3$ and p-fluorobenzoic acid) yielded the correct product but with the presence of an impurity that was later identified by PXRD as nesquehonite ($MgCO_3{\cdot}3H_2O$).[59] Attempts at characterizing this byproduct by ^{25}Mg SSNMR were unsuccessful, as it is known to release CO_2 upon contact with air.[60] Instead, we have synthesized pure Mg(pF) via the reaction of the sodium salt and $MgCl_2$ in a stoichiometric ratio of 1:2 (see Experimental Details for more details).

Our ^{13}C CP/MAS experiments were consistent with the diffraction structures. These spectra, along with those of the pure ligands, are shown in Figure 1 and were acquired at 4.7 or 9.4 T. ^{13}C resonance assignments were aided by field-dependent broadening of some of the resonances due to residual dipolar coupling with nuclei from various functionalities on the aryl ring (i.e., $^{13}C-^{14}N$, $^{13}C-^{35/37}Cl$, $^{13}C-^{19}F$) and by dipolar dephasing experiments at 4.7 T to identify *ipso*-^{13}C resonances.[47] In all cases, the number of ^{13}C carboxyl resonances is consistent with the expected number of magnetically unique carboxylate functionalities present in the crystal structure. Mg(ben) and Mg(pCl) show two carbonyl resonances (for Mg(pCl), $\delta_{iso}(^{13}C{=}O)$ = 176.8 and 172.6 ppm) whereas the other four compounds show only one. This highlights the possibility of differentiating between bridging (Mg−O−C−O−Mg, 176.8 ppm < $\delta_{iso}(^{13}C{=}O)$ < 177.8 ppm) and terminal (Mg−O−C−O, 172.6 ppm < $\delta_{iso}(^{13}C{=}O)$ < 173.9 ppm) carboxylates (see Figure 2) via ^{13}C CP/MAS NMR. Mg(pCl) and Mg(ben) each form one-dimensional polymeric chains with bridging carboxylates, and each Mg^{2+} site is bound to a terminal carboxylate. In Mg(sal) and Mg(pNH$_2$sal), only the terminal type of carboxylate anion is present, so one carbonyl resonance is observed in each spectrum. For Mg(pF), only one type of carboxylate group exists again, but it is of the bridging type in a two-dimensional coordination polymer. This would explain why its chemical shift resembles more closely that of the less shielded carbonyl resonance in Mg(pCl) and Mg(ben) rather than that observed for Mg(sal), for example. The bridging carboxylate moieties tend to have ^{13}C resonances more deshielded than those of the terminal moieties. As for Mg(pNO$_2$), the p−nitrobenzoate ligands are not bound to the magnesium center; thus, an even lower chemical shift is observed for the ^{13}C resonance (170.4 ppm; see Figure 2). It is not possible, however, to distinguish in

dx.doi.org/10.1021/jp405145b | J. Phys. Chem. A 2013, 117, 6561−6570

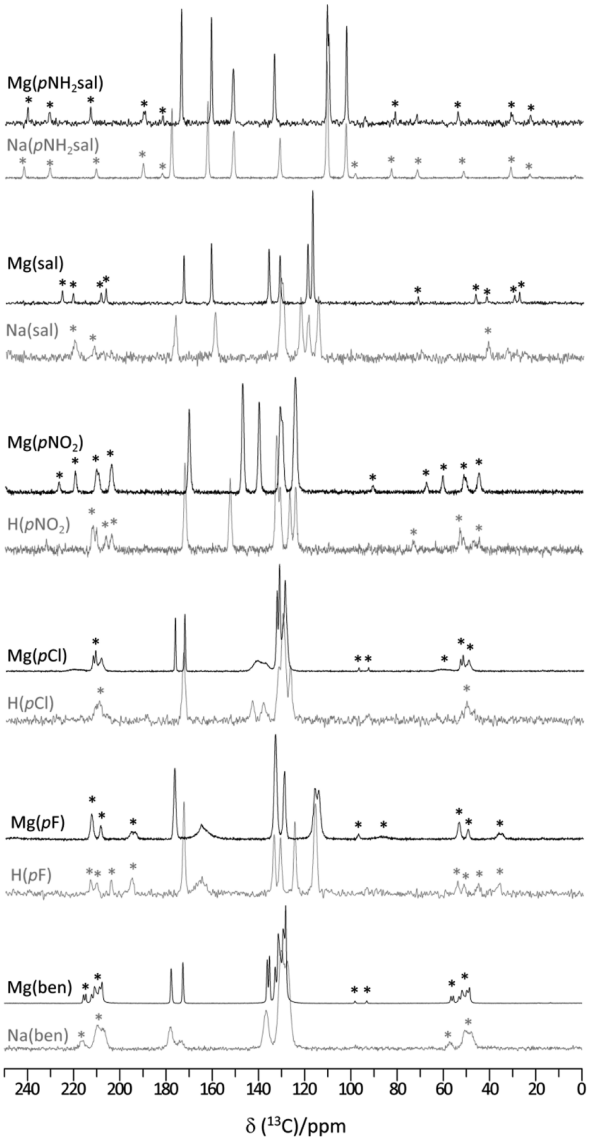

Figure 1. ^{13}C CP/MAS NMR spectra acquired at 4.7 or 9.4 T for all Mg salts (black) characterized in this work along with the spectra of the pure ligands in acid (HL) or sodium salt (NaL) form (gray). A zoomed-in version showing only the carbonyl resonances is given in the Supporting Information (Figure S4).

this case between the chemically equivalent but crystallographically inequivalent "floating" ligands present in the lattice. Such differentiations between different carboxylate binding modes have been observed previously by ^{13}C CP/MAS NMR for zinc clusters.[61,62]

Experimental ^{25}Mg SSNMR of Magnesium Aryl Carboxylates. Presented in Figure 3 are the ^{25}Mg MAS NMR spectra of the magnesium aryl carboxylates considered in this work. All spectra were acquired at B_0 = 21.1 T. These MAS spectra allow for an accurate determination of the ^{25}Mg quadrupolar parameters, C_Q and η_Q, as well as the isotropic chemical shifts, δ_{iso}, in the absence of broadening caused by chemical shift anisotropy (CSA). Complementary NMR spectra acquired under stationary conditions at B_0 = 21.1 T are illustrated in Figure 4. Spectra acquired at B_0 = 9.4 T are shown in the Supporting Information (see Figure S2). We note that at the lower magnetic field strength, we sometimes employed the DFS method to enhance the CT signal via

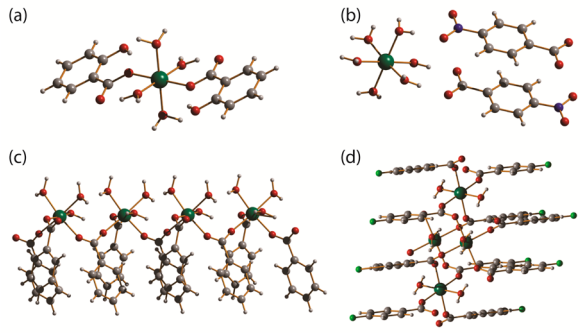

Figure 2. Local crystallographic structures for the magnesium benzoates and salicylates studied in this work. Mg(sal) and Mg(pNH$_2$sal) crystallize similarly in isolated "molecular" coordination units with solely terminal carboxylate ligands as shown in part a for Mg(sal). Mg(pNO$_2$) has a $[Mg(H_2O)_6]^{2+}$ dication and floating p-nitrobenzoate ligands as shown in part b. Mg(ben) and Mg(pCl) crystallize similarly and feature bridging and terminal carboxylate ligands forming a 1D chain as shown for Mg(ben) in part c. Mg(pF) features solely bridging carboxylate ligands, forming a 2D coordination network in part d.

population transfer from the satellite transitions and/or the QCPMG pulse sequence to increase the signal-to-noise ratio. In Table 1 are listed the ^{25}Mg quadrupolar and chemical shift parameters extracted by analytical simulations of the observed line shapes. It was not possible to determine ^{25}Mg CSA at a useful level of precision, as, although its effects on the spectral line shapes are accentuated at higher magnetic field strengths, these are not expected to be larger than ~20 ppm from our calculations (vide infra). This is not surprising given that there are few reported CSA measurements from ^{25}Mg NMR experiments.[40] The observed range in the quadrupolar coupling constant for ^{25}Mg is from 2.70 MHz for Mg(pF) to 6.15 MHz for Mg(pNH$_2$sal), which is consistent with other near-octahedral MgO_6 environments in the handful of reliable data (three compounds) that exist for Mg^{2+} in organic small-molecule environments (i.e., from 2.3 MHz in Mg(HCOO)$_2$·2H$_2$O to 7.1 MHz in Mg(acac)$_2$·2H$_2$O).[39,40] Specific observations made for each compound reported in this work with respect to their individual structures are discussed below.

Structures of Mg Benzoate and Mg *p*-Chlorobenzoate. According to the crystal structure, Mg(ben) crystallizes in the $P2_1/n$ space group and contains two crystallographically distinct Mg^{2+} sites.[41] This is in apparent disagreement with our ^{25}Mg NMR data, as only one site is resolved under MAS and stationary conditions (see Figures 3 and 4) with a $|C_Q(^{25}Mg)|$ of 4.45 MHz and a δ_{iso} of −5 ppm. Although it is conceivable that the two nonequivalent Mg sites could have fortuitously identical ^{25}Mg NMR parameters, this prompted us to redetermine the single-crystal X-ray structure for this compound and we find that Mg(ben) is better described in the $C2/c$ space group. Table 2 contains the relevant unit cell parameters from both structures. It is apparent that the unit cell parameters are very similar to those reported previously, with the main difference being simply the space group used to refine the structure. The new crystal structure has only one unique Mg^{2+} site, consistent with our ^{25}Mg NMR data. Furthermore, we would expect the presence of two terminal as well as two bridging carboxylate resonances in the ^{13}C CP/MAS NMR spectrum if the $P2_1/n$ structure were accurate; instead the

dx.doi.org/10.1021/jp405145b | J. Phys. Chem. A 2013, 117, 6561−6570

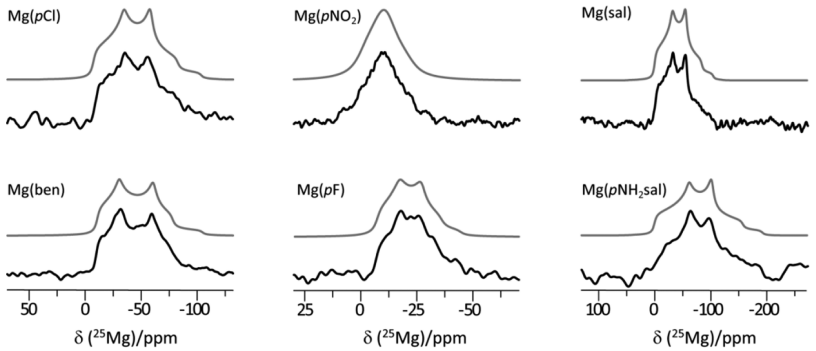

Figure 3. ^{25}Mg MAS NMR spectra acquired at B_0 = 21.1 T. Experimental spectra are in black and analytical simulations are in gray. Spinning frequencies varied from 7 kHz to 12.5 kHz (see Experimental Details).

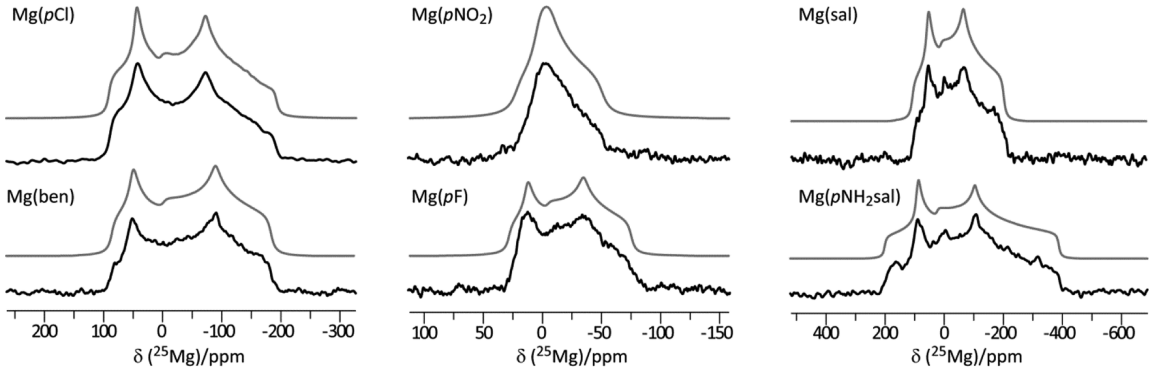

Figure 4. ^{25}Mg NMR spectra acquired at B_0 = 21.1 T under stationary conditions. Experimental spectra are in black, and simulations are in gray. Experiments were performed using a Hahn or solid echo sequence and ^{1}H decoupling (see Experimental Details).

Table 1. Experimental ^{25}Mg EFG Tensor Parameters and Chemical Shifts for Mg Aryl Carboxylates[a]

compound	$\lvert C_Q(^{25}Mg)\rvert$[b], MHz	η_Q	δ_{iso}, ppm
Mg(*p*F)	2.70(0.05)	0.47(0.03)	−5(1)
Mg(*p*Cl)	4.42(0.03)	0.50(0.03)	−4(1)
Mg(ben)	4.45(0.05)	0.35(0.05)	−5(1)
Mg(sal)	4.55(0.05)	0.50(0.05)	3(2)
Mg(*p*NH$_2$sal)	6.15(0.05)	0.58(0.02)	3(2)
Mg(*p*NO$_2$)[c]	2.05(0.05)	0.85(0.05)	−2(2)

[a]Experimental errors are in parentheses. [b]The absolute value of the quadrupolar coupling constant is reported. [c]These values represent the dominant site observed in the ^{25}Mg NMR spectra. It was not possible to unambiguously assign parameters for all three Mg sites in this compound. See Results and Discussion for further details.

Table 2. Select Crystallographic Information for Mg(ben) Compared to a Previously Reported Structure (ref 41)[a]

parameter	previous work	this work
space group	$P2_1/n$	$C2/c$
a, Å	8.8802(16)	8.9061(9)
b, Å	10.4210(18)	10.4274(10)
c, Å	35.019(6)	35.226(4)
α, deg	90.000	90.000
β, deg	97.228(3)	97.477(8)
γ, deg	90.000	90.000
volume, Å^3	3214.9(10)	3243.5(6)
R parameter	0.1163	0.0878

[a]Experimental errors are in parentheses.

spectrum clearly shows only two peaks total in the carboxylate region. The simulated PXRD diffractograms from both crystal structures are indistinguishable. This shows that ^{25}Mg and ^{13}C SSNMR experiments can be useful in providing constraints for the refinement of diffraction-based crystallographic information. Figure S5 in the Supporting Information demonstrates this nicely with the aid of GIPAW DFT calculations. Computed parameters based on the $C2/c$ structure provide better agreement with the experimental MAS spectrum at 21.1 T than do computed parameters based on the $P2_1/n$ model. Further evidence for the validity of the $C2/c$ structure of Mg(ben) comes in the form of a comparison with that of Mg(*p*Cl). The structure of the latter is similar to that of Mg(ben) in that both form the same type of 1D coordination chains linked by carboxylate anions in the solid state along with three Mg-bound H_2O molecules in a *fac* geometry and a disordered water molecule in the lattice (see Figure 2). Both compounds crystallize in the same space group, $C2/c$, and this is further corroborated by their identical $\lvert C_Q(^{25}Mg)\rvert$ and δ_{iso} values within experimental error.

^{25}Mg Chemical Shifts and the Binding Motifs of Aryl Carboxylates. The single-crystal X-ray diffraction structure for Mg(*p*F) has one unique Mg^{2+} site, and this is supported by the observation of a single resonance in the ^{25}Mg NMR spectra with a distinct second-order quadrupolar line shape at 21.1 T (see Figures 3 and 4) and at 9.4 T (see Figure S2). It is not immediately clear why one of the lowest $\lvert C_Q(^{25}Mg)\rvert$ values (2.70 MHz) is observed for this compound, and we note that Mg(*p*F) also has one of the lowest δ_{iso} values of −5 ppm in this study. It has been suggested previously by Smith and co-workers[39] that in general, more strongly hydrated Mg^{2+} ions

dx.doi.org/10.1021/jp405145b | J. Phys. Chem. A 2013, 117, 6561−6570

will tend to have smaller δ_{iso} values. There is an apparent incongruity in our work between Mg(*p*F), which has two H_2O molecules bound to Mg^{2+} and Mg(sal) for example, which has four water molecules coordinated to Mg^{2+} and a larger δ_{iso} of 3 ppm. Furthermore, Mg($p$$NO_2$), in which the magnesium dications are present entirely as $[Mg(H_2O)_6]^{2+}$ units, has a more intermediate isotropic chemical shift of −2 ppm. From our data alone, we can speculate that in general, for near-octahedral MgO_6 units with carboxylate ligands, Mg^{2+} centers that are involved in coordination networks (i.e., 1D chains or 2D sheets) such as Mg(*p*F), Mg(*p*Cl), and Mg(ben) have lower δ_{iso} values than compounds where Mg^{2+} is not part of a coordination network such as in Mg($p$$NO_2$), Mg(sal), and Mg($p$$NH_2$sal). In other words, the isotropic chemical shift for Mg^{2+} in organic molecular environments cannot be related to the hydration state of the compound. Our observations agree with data reported for $Mg(OAc)_2\cdot4H_2O$ and Mg-$(acac)_2\cdot2H_2O$,[40] which form a discrete molecular magnesium complex and have δ_{iso} values of 4.1(0.3) and 2.7(4.0) ppm, respectively. Magnesium formate dihydrate (Mg-$(HCOO)_2\cdot2H_2O$) is not considered here, as different research groups have reported very different experimental values of δ_{iso}.[26]

Significant Range of ^{25}Mg Quadrupolar Coupling Constants. Mg(sal) and Mg($p$$NH_2$sal) both crystallize with discrete magnesium coordination units composed of four water molecules and two carboxylate ligands, which are trans with respect to each other (see Figure 2a). They crystallize in similar space groups (i.e., $P2_1/n$ and $P2_1/a$ for Mg(sal) and Mg($p$$NH_2$sal), respectively). It was somewhat unexpected then that their respective $|C_Q(^{25}Mg)|$ values differ by 35%: 4.55 MHz for Mg(sal) and 6.15 MHz for Mg($p$$NH_2$sal). To investigate this more thoroughly, the inner sphere coordination environments surrounding each Mg^{2+} center were examined, and it is seen that more significant Mg−O distance distortions relative to a perfect octahedron are present in the Mg($p$$NH_2$sal) structure than in Mg(sal) in the form of an elongated octahedron. Despite the structural differences in the organic ligands used in this study, it is therefore possible that the relatively large range in the $|C_Q(^{25}Mg)|$ values may be chiefly attributed to the degree of distortion of the inner sphere MgO_6 octahedra in all of the aryl carboxylate structures. Previous ^{25}Mg studies[27,39] have already postulated such a correlation with respect to the longitudinal strain as proposed by Ghose and Tsang for ^{27}Al studies.[63] They defined this parameter as follows:

$$|\alpha| = \sum_i \left| \ln\left(\frac{l_i}{l_0}\right) \right|$$

where l_i are the experimental Mg−O bond lengths of the octahedron and l_0 is the Mg−O bond length of a perfect octahedron of identical volume to that of the distorted polyhedron. Very recently, this correlation was *not* observed for inorganic magnesium phosphates,[27] but a reasonable correlation between $|C_Q(^{25}Mg)|$ and $|\alpha|$ was noted for a limited data set composed of only $Mg(HCOO)_2\cdot2H_2O$, $Mg(OAc)_2\cdot4H_2O$, and $Mg(acac)_2\cdot2H_2O$.[39] In Figure 5 is plotted our correlation between the C_Q and the longitudinal strains (filled diamonds) for the magnesium aryl carboxylates. Literature data for organic magnesium complexes are also included in the linear regression (white diamonds). This work has doubled the amount of available NMR data for near-octahedral "MgO_6" environments with organic ligands. A clear linear correlation is observed, indicating that the NMR parameters can reflect the geometry in the first coordination sphere of Mg^{2+}. However, more information is necessary if we are to understand why the $|C_Q(^{25}Mg)|$ values in organic complexes correlate with the first coordination sphere structure whereas the values in inorganic compounds cannot be correlated with structure in this fashion. Insights from GIPAW DFT computations, which account for longer-range interactions between Mg^{2+} and its surroundings, will be useful in answering this question.

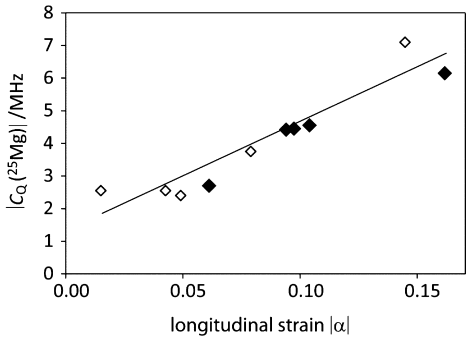

Figure 5. Linear correlation between the experimental $|C_Q(^{25}Mg)|$ values and the longitudinal strain, $|\alpha|$. The filled black diamonds represent data for the magnesium aryl carboxylates in this work, and the empty diamonds represent data for $Mg(HCOO)_2\cdot2H_2O$, Mg-$(OAc)_2\cdot4H_2O$, and $Mg(acac)_2\cdot2H_2O$ from previous studies. Experimental data for Mg($p$$NO_2$) were excluded from the plot because while the crystal structure shows three nonequivalent sites (and longitudinal strains), only a single set of quadrupolar parameters was resolved by ^{25}Mg NMR. Error bars do not exceed the size of the data points. The correlation is $|C_Q(^{25}Mg)| = 33.4|\alpha| + 1.2$ with a correlation coefficient, R, of 0.9435.

GIPAW DFT Computations. The GIPAW DFT method has been used to complement experimental measurements of ^{25}Mg EFG and chemical shift (CS) tensor parameters in crystalline inorganic and organic solids containing magnesium cations.[39,40,64] For instance, these have been used previously for spectral assignment[27] as well as for structure refinement purposes.[65] The GIPAW DFT-calculated EFG and CS tensor parameters for the present work are reported in Table 3. The data show that it would be difficult to observe experimentally the effects of CSA on the ^{25}Mg NMR spectra given that the largest calculated span is only 35 ppm, for Mg($p$$NH_2$sal).

In terms of the reproducibility of experimental NMR parameters with GIPAW DFT computations, the quadrupolar parameters are very well estimated (see Figure 6) for the Mg aryl carboxylates as shown by the slope of 1.16 and correlation coefficient of 0.9923. Across all classes of Mg compounds, an overestimation of $C_Q(^{25}Mg)$ has been observed.[26] For Mg(*p*Cl) and Mg(ben), two different calculations were performed on each compound due to disorder of the unbound water molecule in each of the lattices. For Mg(*p*Cl) and Mg(ben), the calculated $C_Q(^{25}Mg)$ values for different water molecule orientations were within ∼9% of each other. One outlier in our study, however, is evidently Mg($p$$NO_2$), where three chemically distinct Mg sites are present in the lattice with calculated quadrupolar coupling constants of 2.58, 3.66, and 1.95 MHz; only one site is unambiguously distinguishable in the experimental stationary ^{25}Mg NMR spectrum acquired at B_0 = 21.1 T. This can be interpreted initially by the possibility of an average $[Mg(H_2O)_6]^{2+}$ unit that could represent our

dx.doi.org/10.1021/jp405145b | J. Phys. Chem. A 2013, 117, 6561−6570

Table 3. Calculated ^{25}Mg EFG and CS Tensor Parameters for Mg Aryl Carboxylates

compound	$C_Q(^{25}Mg)$, MHz	η_Q	δ_{iso}, ppm[a]	Ω, ppm	κ
Mg(*p*F)	−3.04	0.98	−1	21	0.16
Mg(*p*Cl) − 1[b]	−5.50	0.43	−2	19	0.45
Mg(*p*Cl) − 2[b]	−5.06	0.69	−1	21	0.17
Mg(ben) − 1[b]	−4.82	0.43	−1	16	0.50
Mg(ben) − 2[b]	−4.48	0.60	−2	18	0.21
Mg(sal)	−4.60	0.85	7	19	−0.27
Mg(*p*NH_2sal)	−7.58	0.50	6	35	0.43
Mg(*p*NO_2) − 1[c]	2.58	0.82	7	11	−0.42
Mg(*p*NO_2) − 2[c]	3.66	0.70	6	14	−0.28
Mg(*p*NO_2) − 3[c]	1.95	0.74	7	6	0.06

[a]Chemical shifts were calculated using the absolute shielding constant of Pallister et al. (ref 40). δ_{iso} = (566(1) ppm − σ_{iso})/(1 − 566(1) ppm) [b]There is a disordered floating water molecule in the lattice so two separate calculations were performed for each compound to assess its effect on the calculated NMR parameters. [c]Three crystallographically distinct sites are present in the unit cell of this compound, and it was not possible to resolve them experimentally. For more details, see the main text.

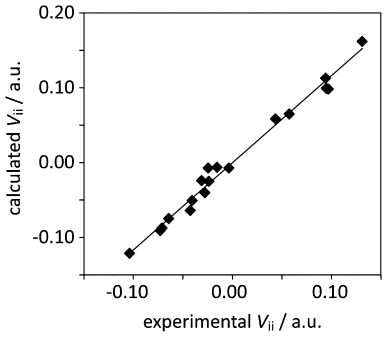

Figure 6. Relationship between the calculated and experimental EFG tensor principal components, V_{ii} (ii = 11, 22, and 33), for all Mg aryl carboxylates reported in this work. The average calculated values for Mg(*p*Cl), Mg(ben), and Mg(*p*NO_2) are represented in this plot (see Table 3). The correlation is described by V_{ii}(calcd) = 1.16V_{ii}(exptl) with a correlation coefficient, *R*, of 0.9923 and a *y* intercept of 0.00.

structure under the current experimental conditions at room temperature because thermal motions of the water molecules are a possibility; the crystal structure was acquired at a temperature of 123 K, and GIPAW DFT computations are typically performed at 0 K. However, after simulating the low-field ^{25}Mg MAS spectrum at 9.4 T (see Figure S2 in the Supporting Information) with the NMR parameters determined from the 21.1 T data, we concluded that it could be difficult to unambiguously observe all three sites experimentally. Natural abundance ^{25}Mg MQMAS NMR spectroscopy could possibly be used to resolve these sites, as has been demonstrated recently in magnesium-containing MOFs.[44] Shown in Figure 7 are comparisons of the analytical simulations of the experimental and GIPAW DFT-calculated NMR spectra. Given the observed line shape of the calculated spectra at both 9.4 and 21.1 T, it is not surprising that the subtle singularities expected at low-field strengths are not present given the low sensitivity of the ^{25}Mg nuclide. As for the 21.1 T simulation, low-intensity singularities are expected for the broader Mg site because of the high calculated quadrupolar asymmetry parameters (see Table 3). Unfortunately, these seem to be

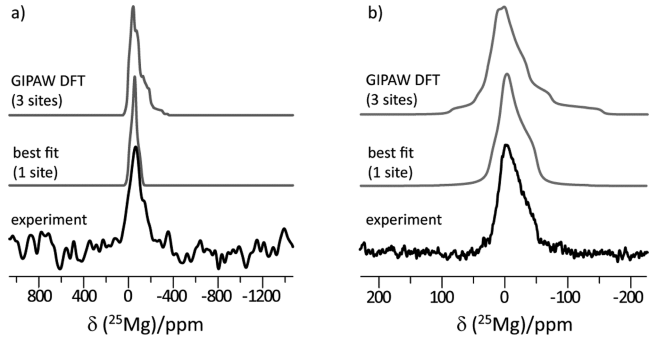

Figure 7. ^{25}Mg MAS (ν_{rot} = 5 kHz) NMR spectrum of Mg(*p*NO_2) at 9.4 T (a) and stationary ^{25}Mg NMR spectrum at 21.1 T (b). The "best fit" simulation is based on the spectrum acquired at 21.1 T. From the 9.4 T experiment, it is clear that one crystallographically unique Mg site does not adequately describe Mg(*p*NO_2). A better description of this system comes from a simulation using the GIPAW DFT-calculated EFG tensor parameters (top traces).

too low in intensity to observe unambiguously, even at 21.1 T. This point highlights the advantages of this experimental−theoretical approach when attempting to corroborate or refine crystal structures, especially when the probe nuclide is as dilute in the samples as in the case of Mg aryl carboxylates.

Another benefit to complementing experimental NMR data with quantum chemical calculations is that theoretical EFG and CS tensor orientations with respect to the crystalline lattice can be obtained. This type of analysis can be advantageous in explaining certain experimental trends in the NMR parameters.[66−70] For ^{25}Mg, the visualization of the EFG tensor with respect to the molecular structure has not been performed in a systematic way. In zirconium silicates for instance,[71] the largest component of the Zr EFG tensor, V_{33}, was calculated by DFT to be oriented along the shortest Zr−O bond in octahedral ZrO_6 units, and the presence of atoms in the second or third coordination sphere of Zr were shown to affect both the magnitudes and directions of the principal components of the EFG tensor. In Table S1 (Supporting Information), we report the calculated values of $C_Q(^{25}Mg)$ along with the orientation of V_{33} with respect to the shortest or longest (i.e., pseudounique) Mg−O bonds in the Mg aryl carboxylates. We note that when the value of $C_Q(^{25}Mg)$ is negative, V_{33} is oriented along the shortest Mg−O bond; when this is positive, V_{33} is along the longest Mg−O bond. An example for Mg(*p*F) is shown in Figure S3. This type of information is often only obtainable via quantum chemical calculations, as it is not possible to evaluate the sign of C_Q experimentally in these systems in any straightforward manner.

Our GIPAW DFT computations suggest that the value of $C_Q(^{25}Mg)$ is positive when "MgO_6" octahedra are present in the form of $[Mg(H_2O)_6]^{2+}$ clusters. To evaluate the validity of this hypothesis, we have performed GIPAW DFT computations on a family of inorganic magnesium compounds that contain $[Mg(H_2O)_6]^{2+}$ units; these are $MgCl_2{\cdot}6H_2O$,[72] $MgSO_4{\cdot}11H_2O$,[73] $Mg(NH_4)_2(SO_4)_2{\cdot}6H_2O$,[74] and $Mg(NO_3)_2{\cdot}6H_2O$.[75] Reported in Table S2 are their respective $C_Q(^{25}Mg)$ values along with the orientation of V_{33} with respect to the longest or shortest Mg−O bond length. It is clear that first, there are changes in the sign of C_Q depending on the compound and that second, V_{33} is not clearly oriented along any Mg−O bond compared to the results from the Mg aryl carboxylates. The latter statement is significant because this

dx.doi.org/10.1021/jp405145b | J. Phys. Chem. A 2013, 117, 6561−6570

provides insight as to why the $C_Q(^{25}Mg)$ values and the longitudinal strain are not as well correlated for inorganic solids[27,39] compared to near-octahedral organic magnesium complexes (see Figure 4). This may be caused by the presence of smaller/harder ions in closer proximity to the Mg^{2+} centers in inorganic solids, resulting in stronger EFGs stemming from the presence of anions in the second or third coordination sphere of Mg^{2+}. As for the benzoates and salicylates in this study for example, the orientations of the EFG tensors are dictated solely by the first coordination sphere possibly because the organic anions are much larger and they diffuse their negative charge through resonance effects. Therefore, geometrical considerations (e.g., longitudinal strain) are enough to explain the breadth in the $C_Q(^{25}Mg)$ values experimentally observed for all of the organic magnesium complexes currently characterized by ^{25}Mg SSNMR.

CONCLUSIONS

We have synthesized a series of six magnesium aryl carboxylates that feature Mg^{2+} in organic coordination environments. These have been characterized by multinuclear (^{13}C and ^{25}Mg) solid-state NMR spectroscopy. It has been demonstrated that the ^{13}C carbonyl resonances are sensitive to the binding mode of the ligand to the Mg dication as characterized by a difference of ~8 ppm between unbound (−O−*C*−O−) and bridging (Mg−O−*C*−O−Mg) carboxylate moieties. The use of an ultrahigh-field magnet (B_0 = 21.1 T) was highly advantageous to obtain high-quality natural abundance ^{25}Mg NMR spectra. ^{25}Mg isotropic chemical shifts were shown to be sensitive to the type of framework of the solid rather than only the hydration state of Mg^{2+} as previously suggested. Lower chemical shifts are observed for the compounds present in 1D chains or 2D sheets, whereas higher chemical shifts are observed for the compounds that crystallize with Mg^{2+} as part of an isolated molecule. A good correlation has been observed between the ^{25}Mg quadrupolar coupling constant and the longitudinal strain of the octahedron formed by the six oxygen atoms present in the first coordination sphere of Mg^{2+} for the compounds in the present study and all other organic Mg-containing compounds for which ^{25}Mg solid-state NMR data already exist. These relationships between the crystal structures and the NMR parameters hold promise for ^{25}Mg solid-state NMR as a tool for refining and optimizing more complex structures such as MOFs. In Mg(ben) for example, the ^{25}Mg NMR data were not consistent with the previously reported structure and a new crystal structure was determined for this compound. GIPAW DFT calculations have also allowed us to visualize the EFG tensor principal components with respect to the molecular structure. We found that the largest component, V_{33}, is oriented along the pseudounique Mg−O bond in the MgO_6 coordination octahedron. This has provided reasoning for the observed relationship between the $C_Q(^{25}Mg)$ values and the longitudinal strain for Mg^{2+} in organic coordination environments compared to the situation for inorganic magnesium compounds.

ASSOCIATED CONTENT

Supporting Information

X-ray diffractograms; additional experimental and computational details; additional spectra and figures; crystallographic information and cif for magnesium benzoate. This material is available free of charge via the Internet at http://pubs.acs.org.

AUTHOR INFORMATION

Corresponding Author

*Tel: +1 613 562 5800 ext. 2018; fax: +1 613 562 5170; e-mail: dbryce@uottawa.ca.

Notes

The authors declare no competing financial interest.

ACKNOWLEDGMENTS

K.M.N.B. and Y.X. thank the Natural Sciences and Engineering Research Council (NSERC) of Canada for graduate and undergraduate scholarships, respectively. D. L. B. thanks NSERC, the Canada Foundation for Innovation, and the Ontario Ministry of Research and Innovation for funding. We thank Dr. Glenn Facey, Dr. Ilia Korobkov, Dr. Tara Kell, and Dr. Victor Terskikh for technical support. Access to the 900 MHz NMR spectrometer was provided by the National Ultrahigh-Field NMR Facility for Solids (Ottawa, Canada), a national research facility funded by the Canada Foundation for Innovation, the Ontario Innovation Trust, Recherche Québec, the National Research Council Canada, and Bruker BioSpin and managed by the University of Ottawa (www.nmr900.ca). NSERC is acknowledged for a Major Resources Support grant.

REFERENCES

(1) Babu, C. S.; Dudev, T.; Lim, C. Differential Role of the Protein Matrix on the Binding of a Catalytic Aspartate to Mg^{2+} vs Ca^{2+}: Application to Ribonuclease H. *J. Am. Chem. Soc.* **2013**, *135*, 6541−6548.

(2) Lim, D.-W.; Yoon, J. W.; Ryu, K. Y.; Suh, M. P. Magnesium Nanocrystals Embedded in a Metal−Organic Framework: Hybrid Hydrogen Storage with Synergistic Effect on Physi- and Chemisorption. *Angew. Chem., Int. Ed.* **2012**, *51*, 9814−9817.

(3) Glover, T. G.; Peterson, G. W.; Schindler, B. J.; Britt, D.; Yaghi, O. MOF-74 Building Unit has a Direct Impact on Toxic Gas Adsorption. *Chem. Eng. Sci.* **2011**, *66*, 163−170.

(4) Kong, X.; Scott, E.; Ding, W.; Mason, J. A.; Long, J. R.; Reimer, J. A. CO_2 Dynamics in a Metal−Organic Framework with Open Metal Sites. *J. Am. Chem. Soc.* **2012**, *134*, 14341−14344.

(5) Lin, L.-C.; Kim, J.; Kong, X.; Scott, E.; McDonald, T. M.; Long, J. R.; Reimer, J. A.; Smit, B. Understanding CO_2 Dynamics in Metal-Organic Frameworks with Open Metal Sites. *Angew. Chem., Int. Ed.* **2013**, *52*, 4410−4413.

(6) Huang, Y.-L.; Gong, Y.-N.; Jiang, L.; Lu, T.-B. A Unique Magnesium-Based 3D MOF with Nanoscale Cages and Temperature Dependent Selective Gas Sorption Properties. *Chem. Commun.* **2013**, *49*, 1753−1755.

(7) Miehé-Brendlé, J.; Tuilier, M.-H.; Marichal, C.; Gallego, J.-C.; Reinholdt, M. Mg Environments in the Octahedral Sheet of 2:1 Talc-Like Hybrid Phyllosilicates: A Comparative XAFS Study. *Eur. J. Inorg. Chem.* **2010**, 5587−5591.

(8) Wasylishen, R. E.; Ashbrook, S. E.; Wimperis, S., Eds. NMR of Quadrupolar Nuclei in Solid Materials; Wiley: Chichester, UK, 2012.

(9) Fernandez, C.; Pruski, M. Probing Quadrupolar Nuclei by Solid-State NMR Spectroscopy: Recent Advances. *Top. Curr. Chem.* **2012**, *306*, 119−188.

(10) Ashbrook, S. E.; Duer, M. J. Structural Information from Quadrupolar Nuclei in Solid State NMR. *Concepts Magn. Reson., Part A* **2006**, *28*, 183−248.

(11) Harris, R. K.; Wasylishen, R. E.; Duer, M. J., Eds. *NMR Crystallography*; Wiley: Chichester UK, 2009.

(12) Perras, F. A.; Bryce, D. L. Multinuclear Magnetic Resonance Crystallographic Structure Refinement and Cross-Validation Using Experimental and Computed Electric Field Gradients: Application to $Na_2Al_2B_2O_7$. *J. Phys. Chem. C* **2012**, *116*, 19472−19482.

(13) Santos, S. M.; Rocha, J.; Mafra, L. NMR Crystallography: Toward Chemical Shift-Driven Crystal Structure Determination of the

β-Lactam Antibiotic Amoxicillin Trihydrate. *Cryst. Growth. Des.* **2013**, *13* (6), 2390−2395.
(14) Pawlak, T.; Jaworska, M.; Potrzebowski, M. J. NMR Crystallography of α-Poly(L-lactide). *Phys. Chem. Chem. Phys.* **2013**, *15*, 3137−3145.
(15) Brouwer, D. H.; Cadars, S.; Eckert, J.; Liu, Z.; Terasaki, O.; Chmelka, B. F. A General Protocol for Determining the Structures of Molecularly Ordered but Noncrystalline Silicate Frameworks. *J. Am. Chem. Soc.* **2013**, *135*, 5641−5655.
(16) Macholl, S.; Börner, F.; Buntkowsky, G. Revealing the Configuration and Crystal Packing of Organic Compounds by Solid-State NMR Spectroscopy: Methoxycarbonylurea, a Case Study. *Chem.—Eur. J.* **2004**, *10*, 4808−4816.
(17) Elena, B.; Emsley, L. Powder Crystallography by Proton Solid-State NMR Spectroscopy. *J. Am. Chem. Soc.* **2005**, *127*, 9140−9146.
(18) Elena, B.; Pintacuda, G.; Mifsud, N.; Emsley, L. Molecular Structure Determination in Powders by NMR Crystallography from Proton Spin Diffusion. *J. Am. Chem. Soc.* **2006**, *128*, 9555−9560.
(19) Pickard, C. J.; Salager, E.; Pintacuda, G.; Elena, B.; Emsley, L. Resolving Structures from Powders by NMR Crystallography Using Combined Proton Spin Diffusion and Plane Wave DFT Calculations. *J. Am. Chem. Soc.* **2007**, *129*, 8932−8933.
(20) Dutour, J.; Guillou, N.; Huguenard, C.; Taulelle, F.; Mellot-Draznieks, C.; Férey, G. Chiolite, A Case Study for Combining NMR Crystallography, Diffraction and Structural Simulation. *Solid State Sci.* **2004**, *6*, 1059−1067.
(21) Bouchevreau, B.; Martineau, C.; Mellot-Draznieks, C.; Tuel, A.; Suchomel, M. R.; Trébosc, J.; Lafon, O.; Amoureux, J.-P.; Taulelle, F. An NMR-Driven Crystallography Strategy to Overcome the Computability Limit of Powder Structure Determination: A Layered Aluminophosphate Case. *Chem.—Eur. J.* **2013**, *19*, 5009−5013.
(22) Brouwer, D. H. NMR Crystallography of Zeolites: Refinement of an NMR-Solved Crystal Structure Using ab Initio Calculations of ^{29}Si Chemical Shift Tensors. *J. Am. Chem. Soc.* **2008**, *130*, 6306−6307.
(23) Brouwer, D. H.; Enright, G. D. Probing Local Structure in Zeolite Frameworks: Ultrahigh-Field NMR Measurements and Accurate First-Principles Calculations of Zeolite ^{29}Si Magnetic Shielding Tensors. *J. Am. Chem. Soc.* **2008**, *130*, 3095−3105.
(24) Brouwer, D. H. A Structure Refinement Strategy for NMR Crystallography: An Improved Crystal Structure of Silica-ZSM-12 Zeolite from ^{29}Si Chemical Shift Tensors. *J. Magn. Reson.* **2008**, *194*, 136−146.
(25) Pyykkö, P. Year-2008 Nuclear Quadrupole Moments. *Mol. Phys.* **2008**, *106*, 1965−1974.
(26) Freitas, J. C. C.; Smith, M. E. Recent Advances in Solid-State ^{25}Mg NMR Spectroscopy. *Annu. Rep. Nucl. Magn. Reson. Spectrosc.* **2012**, *75*, 25−114.
(27) Laurencin, D.; Gervais, C.; Stork, H.; Krämer, S.; Massiot, D.; Fayon, F. ^{25}Mg Solid-State NMR of Magnesium Phosphates: High Magnetic Field Experiments and Density Functional Theory Calculations. *J. Phys. Chem. C* **2012**, *116*, 19984−19995.
(28) Sham, S.; Wu, G. Solid-State ^{25}Mg NMR Study of Inner-Sphere Mg^{2+} Binding Complexes. *Inorg. Chem.* **2000**, *39*, 4−5.
(29) Wu, G.; Wong, A.; Wang, S. Solid-State ^{25}Mg NMR, X-ray Crystallographic, and Quantum Mechanical Study of Bis(pyridine)-(5,10,15,20-tetraphenylporphyrinato)magnesium(II). *Can. J. Chem.* **2003**, *81*, 275−283.
(30) Wong, A.; Ida, R.; Mo, X.; Gan, Z.; Poh, J.; Wu, G. Solid-State ^{25}Mg NMR Spectroscopic and Computational Studies of Organic Compounds. Square-Pyramidal Magnesium(II) Ions in Aqua-(magnesium) Phthalocyanine and Chlorophyll *a*. *J. Phys. Chem. A* **2006**, *110*, 10084−10090.
(31) Lipton, A. S.; Heck, R. W.; Primak, S.; McNeill, D. R.; Wilson, D. M., III; Ellis, P. D. Characterization of Mg^{2+} Binding to the DNA Repair Protein Apurinic/Apyrimidic Endonuclease 1 via Solid-State ^{25}Mg NMR Spectroscopy. *J. Am. Chem. Soc.* **2008**, *130*, 9332−9341.
(32) Perras, F. A.; Viger-Gravel, J.; Burgess, K. M. N.; Bryce, D. L. Signal Enhancement in Solid-State NMR of Quadrupolar Nuclei. *Solid State Nucl. Magn. Reson.* **2013**, *51*−*52*, 1−15.
(33) Siegel, R.; Nakashima, T. T.; Wasylishen, R. E. Sensitivity Enhancement of NMR Spectra of Half-Integer Spin Quadrupolar Nuclei in Solids using Hyperbolic Secant Pulses. *J. Magn. Reson.* **2007**, *184*, 85−100.
(34) Kentgens, A. P. M.; Verhagen, R. Advantages of Double frequency Sweeps in Static, MAS and MQMAS NMR of Spin I=3/2 Nuclei. *Chem. Phys. Lett.* **1999**, *300*, 435−443.
(35) Iuga, D.; Schäfer, H.; Verhagen, R.; Kentgens, A. P. M. Population and Coherence Transfer Induced by Double Frequency Sweeps in Half-Integer Quadrupolar Spin Systems. *J. Magn. Reson.* **2000**, *147*, 192−209.
(36) Freitas, J. C. C.; Wong, A.; Smith, M. E. Solid-State Natural Abundance ^{25}Mg NMR Studies of $Na_2MgEDTA{\cdot}4H_2O$ − A Possible New Reference Compound for ^{25}Mg NMR Spectroscopy. *Magn. Reson. Chem.* **2009**, *47*, 9−15.
(37) Cheng, J. T.; Ellis, P. D. Adsorption of Rb^+ to γ-alumina as Followed by Solid-State Rubidium-87 NMR Spectroscopy. *J. Phys. Chem.* **1989**, *93*, 2549−2555.
(38) Larsen, F. H.; Skibsted, J.; Jakobsen, H. J.; Nielsen, N. C. Solid-State QCPMG NMR of Low-γ Quadrupolar Metal Nuclei in Natural Abundance. *J. Am. Chem. Soc.* **2000**, *122*, 7080−7086.
(39) Cahill, L. S.; Hanna, J. V.; Wong, A.; Freitas, J. C. C.; Yates, J. R.; Harris, R. K.; Smith, M. E. Natural Abundance ^{25}Mg Solid-State NMR of Mg Oxyanion Systems: A Combined Experimental and Computational Study. *Chem.—Eur. J.* **2009**, *15*, 9785−9798.
(40) Pallister, P. J.; Moudrakovski, I. L.; Ripmeester, J. A. Mg-25 Ultra-High Field Solid State NMR Spectroscopy and First Principles Calculations of Magnesium Compounds. *Phys. Chem. Chem. Phys.* **2009**, *11*, 11487−11500.
(41) Arlin, J.-B.; Florence, A. J.; Johnston, A.; Kennedy, A. R.; Miller, G. J.; Patterson, K. Systematic Data Set for Structure-Property Investigations: Solubility and Solid-State Structure of Alkaline Earth Metal Salts of Benzoates. *Cryst. Growth Des.* **2011**, *11*, 1318−1327.
(42) Zhang, Z.; Zhao, Y.; Gong, Q.; Li, Z.; Li, J. MOFs for CO_2 Capture and Separation from Flue Gas Mixtures: The Effect of Multifunctional Sites on their Adsorption Capacity and Selectivity. *Chem. Commun.* **2013**, *49*, 653−661.
(43) Xu, J.; Terskikh, V. V.; Huang, Y. ^{25}Mg Solid-State NMR: A Sensitive Probe of Adsorbing Guest Molecules on a Metal Center in Metal−Organic Framework CPO-27-Mg. *J. Phys. Chem. Lett.* **2013**, *4*, 7−11.
(44) Xu, J.; Terskikh, V. V.; Huang, Y. Resolving Multiple Non-equivalent Metal Sites in Magnesium-Containing Metal−Organic Frameworks by Natural Abundance ^{25}Mg Solid-State NMR Spectroscopy. *Chem.—Eur. J.* **2013**, *19*, 4432−4436.
(45) Charpentier, T. The PAW/GIPAW Approach for Computing NMR Parameters: A New Dimension Added to NMR Study of Solids. *Solid State Nucl. Magn. Reson.* **2011**, *40*, 1−20.
(46) Bonhomme, C.; Gervais, C.; Babonneau, F.; Coelho, C.; Pourpoint, F.; Azaïs, T.; Ashbrook, S. E.; Griffin, J. M.; Yates, J. R.; Mauri, F.; Pickard, C. J. First-Principles Calculation of NMR Parameters Using the Gauge Including Projector Augmented Wave Method: A Chemist's Point of View. *Chem. Rev.* **2012**, *112*, 5733−5779.
(47) Opella, S. J.; Frey, M. H. Selection of Nonprotonated Carbon Resonances in Solid-State Nuclear Magnetic Resonance. *J. Am. Chem. Soc.* **1979**, *101*, 5854−5856.
(48) Solomon, I. Multiple Echoes in Solids. *Phys. Rev.* **1958**, *110*, 61−65.
(49) Hartmann, S. R.; Hahn, E. L. Nuclear Double Resonance in the Rotating Frame. *Phys. Rev.* **1962**, *128*, 2042−2053.
(50) Massiot, D.; Farnan, I.; Gautier, N.; Trumeau, D.; Trokiner, A.; Coutures, J. P. ^{71}Ga and ^{69}Ga Nuclear Magnetic Resonance Study of β-Ga_2O_3: Resolution of Four- and Six-fold Coordinated Ga Sites in Static Conditions. *Solid State Nucl. Magn. Reson.* **1995**, *4*, 241−248.
(51) Eichele, K.; Wasylishen, R. E. *WSOLIDS NMR Simulation Software Version 1.17.30*, Universitat Tübingen, Tübingen, Germany, 2001.

(52) Bak, M.; Rasmussen, J. T.; Nielsen, N. C. SIMPSON: A General Simulation Program for Solid-State NMR Spectroscopy. *J. Magn. Reson.* **2000**, *147*, 296−330.
(53) Massiot, D.; Fayon, F.; Capron, M.; King, I.; Le Calvé, S.; Alonso, B.; Durand, J.-O.; Bujoli, B.; Gan, Z.; Hoatson, G. Modelling One- and Two-dimensional Solid-State NMR Spectra. *Magn. Reson. Chem.* **2002**, *40*, 70−76.
(54) Segall, M. D.; Lindan, P. J. D.; Probert, M. J.; Pickard, C. J.; Hasnip, P. J.; Clark, S. J.; Payne, M. C. First-Principles Simulation: Ideas, Illustrations and the CASTEP Code. *J. Phys.: Condens. Matter* **2002**, *14*, 2717−2744.
(55) Perdew, J. P.; Burke, K.; Ernzerhof, M. Generalized Gradient Approximation Made Simple. *Phys. Rev. Lett.* **1996**, *77*, 3865−3868.
(56) Adiga, S.; Aebi, D.; Bryce, D. L. EFGShield — A Program for Parsing and Summarizing the Results of Electric Field Gradient and Nuclear Magnetic Shielding Tensor Calculations. *Can. J. Chem.* **2007**, *85*, 496−505.
(57) Cole, L. B.; Holt, E. M. Alkali and Alkaline Earth Complexation to Derivatives of Salicylic Acid: [Calcium(*p*-aminosalicylate)(acetate)-(H_2O)](H_2O), Magnesium(salicylate)$_2$(H_2O)$_4$, Magnesium(*p*-aminosalicylate)$_2$(H_2O)$_4$, Magnesium(2,6-pyridinedicarboxylate)-(H_2O)$_3$(H_2O)$_2$ and Sodium(*p*-aminosalicylate)(H_2O)$_2$. *Inorg. Chim. Acta* **1989**, *160*, 195−203.
(58) Drake, S. R.; Sanderson, K. D.; Hursthouse, M. B.; Malik, K. M. A. Intensive Hydrogen Bonding in a Monomeric Magnesium Salicylate Tetrahydrate. *Inorg. Chem.* **1993**, *32*, 1041−1044.
(59) Felmy, A. R.; Qafoku, O.; Arey, B. W.; Hu, J. Z.; Hu, M.; Schaef, H. T.; Ilton, E. S.; Hess, N. J.; Pearce, C. I.; Feng, J.; Rosso, K. M. Reaction of Water-Saturated Supercritical CO_2 with Forsterite: Evidence for Magnesite Formation at Low Temperatures. *Geochim. Cosmochim. Acta* **2012**, *91*, 271−282.
(60) Hopkinson, L.; Rutt, K.; Cressey, G. The Transformation of Nesquehonite to Hydromagnesite in the System CaO-MgO-H_2O-CO_2: An Experimental Spectroscopic Study. *J. Geol.* **2008**, *116*, 387−400.
(61) Patra, A.; Sen, T. K.; Bhattacharyya, R.; Mandal, S. K.; Bera, M. Diversity of Carboxylate Binding in a New Tetranuclear Zinc Cluster: Correlation Between Spectroscopic Investigations and Carboxylate Binding Modes. *RSC Adv.* **2012**, *2*, 1774−1777.
(62) Ye, B.-H.; Li, X.-Y.; Williams, I. D.; Chen, X.-M. Synthesis and Structural Characterization of Di- and Tetranuclear Zinc Complexes with Phenolate and Carboxylate Bridges. Correlations between ^{13}C NMR Chemical Shifts and Carboxylate Binding Modes. *Inorg. Chem.* **2002**, *41*, 6426−6431.
(63) Ghose, S.; Tsang, T. Structural Dependence of Quadrupole Coupling Constant e^2qQ/h for ^{27}Al and Crystal Field Parameter D for Fe^{3+} in Aluminosilicates. *Am. Mineral.* **1973**, *58*, 748−755.
(64) Rossano, S.; Mauri, F.; Pickard, C. J.; Farnan, I. First-Principles Calculation of ^{17}O and ^{25}Mg NMR Shieldings in MgO at Finite Temperature: Rovibrational Effect in Solids. *J. Phys. Chem. B* **2005**, *109*, 7245−7250.
(65) Widdifield, C. M.; Bryce, D. L. Crystallographic Structure Refinement with Quadrupolar Nuclei: A Combined Solid-State NMR and GIPAW DFT Example using $MgBr_2$. *Phys. Chem. Chem. Phys.* **2009**, *11*, 7120−7122.
(66) O'Dell, L. A.; Moudrakovski, I. L. A Combined Ultra-Wideline Solid-State NMR and DFT Study of ^{137}Ba Electric Field Gradient Tensors in Barium Compounds. *Chem. Phys. Lett.* **2013**, *565*, 56−60.
(67) Johnston, K. E.; Mitchell, M. R.; Blanc, F.; Lightfoot, P.; Ashbrook, S. E. Structural Study of $La_{1-x}Y_xScO_3$, Combining Neutron Diffraction, Solid-State NMR, and First-Principles DFT Calculations. *J. Phys. Chem. C* **2013**, *117*, 2252−2265.
(68) Burgess, K. M. N.; Korobkov, I.; Bryce, D. L. A Combined Solid-State NMR and X-ray Crystallography Study of the Bromide Anion Environments in Triphenylphosphonium Bromides. *Chem.—Eur. J.* **2012**, *18*, 5748−5758.
(69) Widdifield, C. M.; Bryce, D. L. Solid-State ^{127}I NMR and GIPAW DFT Study of Metal Iodides and Their Hydrates: Structure, Symmetry, and Higher-Order Quadrupole-Induced Effects. *J. Phys. Chem. A* **2010**, *114*, 10810−10823.
(70) Bryce, D. L.; Bultz, E. B.; Aebi, D. Calcium-43 Chemical Shift Tensors as Probes of Calcium Binding Environments. Insight into the Structure of the Vaterite $CaCO_3$ Polymorph by ^{43}Ca Solid-State NMR Spectroscopy. *J. Am. Chem. Soc.* **2008**, *130*, 9282−9292.
(71) Zhu, J.; Lin, Z.; Yan, Z.; Huang, Y. ^{91}Zr and ^{25}Mg Solid-State NMR Characterization of the Local Environments of the Metal Centers in Microporous Materials. *Chem. Phys. Lett.* **2008**, *461*, 260−265.
(72) Agron, P. A.; Busing, W. R. Magnesium Dichloride Hexahydrate, $MgCl_2·6H_2O$, by Neutron Diffraction. *Acta Crystallogr. C* **1985**, *41*, 8−10.
(73) Geneceli, F. E.; Lutz, M.; Spek, A. L.; Witkamp, G.-J. Crystallization and Characterization of a New Magnesium Sulfate Hydrate $MgSO_4·11H_2O$. *Cryst. Growth Des.* **2007**, *7*, 2460−2466.
(74) Margulis, T. N.; Templeton, D. H. Crystal Structure and Hydrogen Bonding of Magnesium Ammonium Sulfate Hexahydrate. *Z. Kristallogr.* **1962**, *117*, 344−357.
(75) Braibanti, A.; Tiripicchio, A.; Lanfredi, A. M. M.; Bigoli, F. The Crystal Structures of Nitrates of Divalent Hexaquocations. II. Hexaquomagnesium Nitrate. *Acta Crystallogr., Sect. B: Struct. Crystallogr. Cryst. Chem.* **1969**, *25*, 354−361.